An analytical model of the equilibrium distribution of suspended sediment in an estuary

S.A. Talke
Institute for Marine and Atmospheric research, Utrecht University, Utrecht, Netherlands

H.E. de Swart
Institute for Marine and Atmospheric research, Utrecht University, Utrecht, Netherlands

H.M. Schuttelaars
Delft Institute of Applied Mathematics/Mathematical Physics, Delft University of Technology, Delft, Netherlands

ABSTRACT:

An analytical solution of the equilibrium distribution of suspended sediment concentrations (SSC) in an estuary along the longitudinal axis is extended to include variable width. A turbidity maximum is formed at the convergence of fluxes from freshwater discharge and (vertically well mixed) salinity gradients. Simple scaling relationships control the longitudinal distribution of SSC and depend upon model parameters such as the applied salinity field, depth, width, freshwater discharge, settling velocity, eddy viscosity, and horizontal dispersion. These scaling relationships agree well with turbidity data from the Ems estuary. The modelled dependence of the SSC distribution on settling velocity (grain size) causes particles with a small settling velocity to be found preferentially in the outer estuary, while particles with a large settling velocity (large grained sand, cohesive sediments) are trapped in the turbid zone.

1 INTRODUCTION

The classical model for an estuarine turbidity maximum holds that tidally averaged gravitational circulation is balanced by freshwater discharge near the toe of the salt wedge, forming a convergence zone in which suspended sediment is trapped (Hansen & Rattray, 1965; Festa & Hansen, 1978). Based on field measurements in the Gironde estuary, Sottolichio & Castaing (1999) posit that variations in width also provide a trapping mechanism for sediments. To investigate the effect of varying width, we extend an existing analytical model of tidally averaged estuarine circulation and sediment distribution (Talke et al., 2007) to include the effect of an exponentially varying width. We then investigate how the distribution of suspended sediment concentration (SSC) changes as width, depth, mixing, settling velocity, and other model parameters vary. By deducing length-scales that control the upstream and downstream profile of SSC, we explain the mechanisms that control the size and asymmetry of a turbid zone. In turn, these length scales indicate how the distribution of SSC depends on settling velocity. The nonlinear variation of SSC distribution on settling velocity provides a mechanism for the sorting of sediments in an estuary. In the following sections we present the model in section 2, analyze results in section 3, and draw conclusions section 4.

2 MODEL SETUP

The model applies the rigid lid and Boussinesq assumptions, and assumes that settling velocity, eddy viscosity, eddy diffusivity, and longitudinal dispersion are constant throughout the model domain. Freshwater discharge is held constant, while the salinity is assumed to be well mixed vertically and described longitudinally by a prescribed hyperbolic tangent:

$$s(x) = 0.5 S_* \left\{ 1 - \tanh\left(\frac{x - x_c}{x_L} \right) \right\} \quad (1)$$

where S_* [psu] is the maximum salinity, x_c [m] is the position of the maximum salinity gradient, and x_L [m] scales the salinity gradient. The x-axis points in the along-estuary (upstream) direction. Furthermore, the z-axis points vertically upward, with $z = 0$ the undisturbed water level and $z = -H$ the bed level. Velocity components u and w are defined along the x and z axes, respectively. Using scaling analysis, we find that the momentum balance from Talke et al. (2007) remains unchanged when width varies smoothly. Because of their corresponding small magnitude, nonlinear terms such as $u\,\partial u/\partial x$ and $w\partial u/\partial z$ are neglected, and the tidally averaged momentum equation reads:

$$0 = -g\int_{-H}^{z}\frac{\partial\rho}{\partial x}dz' + g\rho\frac{d\eta}{dx} + \frac{\partial}{\partial z}\left\{\rho_o A_v\frac{\partial u}{\partial z}\right\} \quad (2)$$

where g is gravity [m/s^2], ρ is the density [kg/m^3], η is the surface slope [-], and A_z is the eddy viscosity [m^2/s]. To the momentum equation we apply the no-slip boundary condition at the bottom and assume no wind shear at the surface. We define the density ρ as a function of both the salinity $s(x)$ and the suspended sediment concentration $C(x,z)$:

$$\rho(x,z) = \rho_w + \beta s(x) + \gamma C(x,z), \quad (3)$$

in which ρ_w is the density of water. The factors $\beta \sim 0.83$ kg/m^3/psu and $\gamma = (\rho_s - \rho_w)/\rho_s \sim 0.62$ convert, respectively, salinity and SSC into density, where ρ_s is the density of fine-grained sand particles. To determine the residual current structure, we next apply mass balance for water. This requires that the total flow through a cross-section equals the prescribed freshwater discharge Q [m^3/s]:

$$\int_{-H}^{0} u(x,z)b(x)dz = Q \quad (4)$$

where $u(x,z)$ is the tidally averaged current and H and $b(x)$ are the depth and width at a position x. Note that Q is a negative quantity in our coordinate system.

As in Talke et al. (2007), we assume that the downwards settling flux of particles is balanced by the upwards diffusion of sediment, which yields an exponential profile of SSC in the vertical direction:

$$c(x,z) = C_b(x)\exp\left\{\frac{-w_s}{K_v}(z+H)\right\} \quad (5)$$

where w_s [m/s] is the settling velocity, K_v [m^2/s] is the constant eddy diffusivity, and $C_b(x)$ is the (to be solved for) suspended sediment concentration at the bed. Eqs. 1-5 are solved to yield an expression for the tidally averaged circulation structure as a function of the bottom concentration $C_b(x)$. When gradients of SSC are negligible, the residual currents are described by the traditional relations for gravitational circulation (e.g., Officer, 1976). When turbidity gradients are on the same order of magnitude as salinity gradients, the solution for residual circulation described in Talke et al. (2007) is applied.

To solve for the equilibrium distribution of SSC, we apply the condition of morphodynamic equilibrium, which states that the vertically integrated flux of sediment over a cross-section vanishes during equilibrium conditions:

$$\int_{-H}^{0}\int_{-b/2}^{b/2}\left\{uC - K_h\frac{\partial C}{\partial x}\right\}dzdy = 0 \quad (6)$$

in which K_h [m^2/s] is the horizontal dispersion coefficient. Assuming that SSC is evenly distributed in the lateral (y) direction, we solve Eq. 6 to yield the following differential equation for the longitudinal distribution of suspended sediment, $C_b(x)$:

$$\frac{dC_b}{dx} = \frac{-J_1(x)C_b(x)}{J_2 C_b(x) + J_3} \quad (7)$$

The full expressions for $J_1(x)$, J_2, and J_3 used in this paper are

$$J_1(x) = -T_s\frac{g\beta H^3}{48\rho_o A_v}\frac{ds}{dx}(x) + \frac{3}{2}T_Q\frac{Q}{Hb(x)} \quad (8)$$

$$J_2 = -T_T\frac{g\gamma H^3}{48\rho_o A_v} \quad (9)$$

$$J_3 = -T_K K_h \quad (10)$$

where $J_1(x)$ describes the vertically integrated effect of salinity gradients and freshwater flow on sediment fluxes, J_2 describes the effect of turbidity currents on vertically integrated fluxes, and J_3 describes the vertically integrated effect of horizontal dispersion on fluxes. The parameters T_S, T_T, T_Q, and T_K are defined in the appendix and are functions of $Pe_v = w_s H/K_v$, where Pe_v is the vertical Peclet number for suspended sediment concentration. The model is closed by defining a constant mass of bottom sediment available for resuspension, and an equation defining the width variation $b(x)$ in the estuary:

$$c_* = \frac{1}{L\langle b\rangle}\int_0^L C_b(x)b(x)dx \quad (11)$$

$$b(x) = B_0\exp(-x/L_e) \quad (12)$$

where L [m] is the length of the model domain, c_* [kg/m^3] is the average bottom SSC, $\langle b\rangle$ is the average width of the domain, B_o[m] is the width at the estuarine mouth, and L_e [m] is the lengthscale of convergence. The set of twelve equations (Eqs. 1-12) are solved to yield the following implicit equation for the distribution of SSC at the bed:

$$C_b(x) = A_1\exp\{F(x)\}, \quad (13a,b)$$

$$F(x) = \frac{-T_s g\beta H^3 s(x)}{48\rho_o A_v T_K K_h} + \frac{3T_Q Q L_e\exp(x/L_e)}{2HT_K K_h B_o} + \frac{J_2 C_b(x)}{T_k K_h}$$

and A_1 is a constant of integration. The first term of $F(x)$ describes the effect of gravitational circulation on the sediment distribution, the second term describes the effect of freshwater discharge, while the third term describes the effect of turbidity currents. Applying Eq. 11, we find that the constant A_1 is a function of the average SSC in the domain, c_*:

$$A_1 = \frac{c_* < b > L}{B_o \int_o^L \exp(-x/L_e) \exp\{F(x)\}\, dx} \qquad (14)$$

3 RESULTS

Fig. 1 shows a plot of the bottom sediment concentration C_b in both a constant width model (in which $L_e \rightarrow \infty$ and $<b>$ = 2500 m) and an exponential width model for the case that c_* is small (default of 0.1 kg/m^3), c_* is large (350 kg/m^3), and c_* is an intermediate value in-between (5 kg/m^3). The values described in Table 1 are used for all other parameters. To allow for comparison, the concentration of each model run is normalized by the maximum SSC.

When c_* is small, the maximum SSC is 0.24 kg/m^3 (constant width model) and 0.97 kg/m^3 (exponential width model). The resulting small SSC gradients result in a negligible affect of turbidity currents (Eq. 9) on sediment fluxes, and the effect of dispersion (Eq. 10) dominates the morphodynamic equilibrium (Eq. 7). When c_* is large, the maximum SSC is 469 kg/m^3 (constant width model) and 507 kg/m^3 (exponential width model). The resulting large SSC gradients cause turbidity currents (Eq. 9) to dominate over the affect of dispersion (Eq. 10) in the morphodynamic equilibrium (Eq. 7).

The intermediate case (c_* = 5 kg/m^3) shows the situation in which both dispersion and turbidity currents may play a role. For a constant width model, the equilibrium distribution of SSC (maximum SSC = 11.6 kg/m^3) results in a profile that is nearly identical with dispersion dominated conditions, indicating negligible turbidity currents. By contrast, the SSC distribution of the exponential width model (maximum SSC = 38.5 kg/m^3) is distinct from dispersion dominated conditions, and shows the additional spreading that turbidity currents provide.

Fig. 1 shows that turbidity currents can be neglected for all but the muddiest estuaries such as the Ems, where bottom SSC larger than 50 kg/m^3 has been observed (see Talke et al., 2007). Essentially this means that for the standard parameter values in this paper (Table 1), dispersive fluxes carry sediment away from the turbidity maximum.

3.1 *Sensitivity Study*

Fig. 2 shows results of a sensitivity study in which the length scale of width convergence L_e and the width at the estuary mouth B_o are varied, with all other parameters held constant. The longitudinal profiles of SSC are normalized by the maximum concentration to allow comparison. As both L_e and B_o increase, the flux balance at the turbidity maximum (set by J_1 =0 in Eq. 8) is altered and the turbid B_o increase, the flux balance at the turbidity maximum (set by J_1 =0 in Eq. 8) is altered and the turb-

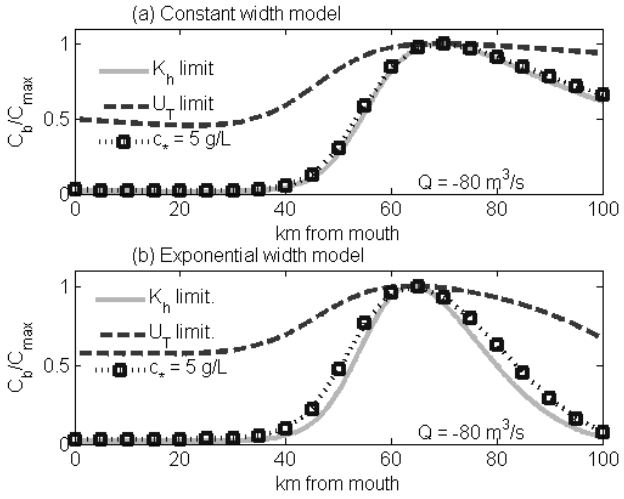

Figure 1. Bottom sediment concentration for c_* =0.1 kg/m^3 (K_h limit), c_* =350 kg/m^3 (U_T limit), and c_* =5 kg/m^3 for both a constant width model (a) and exponential width model (b). A width of 2500 m is used for the constant-width model.

Table 1: Default parameters used to calculate the equilibrium distribution of sediment. The parameters describing the salinity field, flow discharge, depth and the width are average conditions for the Ems estuary (see Talke et al, 2007). The tidally averaged dispersion, diffusivity, and viscosity estimates are typical order of magnitude estimates found in estuaries.

Description	Parameter	Default Value	Units
Salinity Scale	S_*	25.1	psu
Lengthscale salinity gradient	x_L	25,000	m
Position maximum salinity gradient	x_c	46,000	m
Eddy Viscosity	A_v	0.001	m^2/s
Eddy Diffusivity	K_v	0.001	m^2/s
Settling Velocity	w_s	0.001	m/s
Depth	H	7	m
Freshwater Discharge	Q	-80	m^3/s
Dispersion Coefficient	K_h	100	m^2/s
Average sediment concentration	c_*	0.1	kg/m^3
Convergence lengthscale estuarine width	L_e	25,000	m
Width of estuary at entrance	B_o	15,000	m
Model Length	L	100,000	m

ity maximum moves further from the estuarine mouth. The shape of the SSC distribution varies as well, with the largest asymmetry and breadth occurring for large L_e and B_o. Hence sharp variations in width—as occurs for small values of L_e—appear to result in a reduced spatial distribution of turbidity. This is consistent with Sottolichio & Castaing (1999), who posit sharp variations in channel width as a trapping mechanism.

Fig. 3 shows the results of a sensitivity study in which eight additional model parameters are varied, using standard model parameters displayed in Table 1. Note that for comparison purposes, Fig. 3a and 3b are normalized by the maximum SSC, while the other figures are presented in units of kg/m^3.

The results in Fig. 3 show that position of the turbidity maximum and the distribution of SSC are quite sensitive to model parameters in an exponentially converging estuary. Both increasing sediment supply (Fig. 3a) and greater dispersion (Fig. 3b) cause an increased spread in the turbid zone, but do not affect the position of the turbidity maximum. The increased spread reduces the maximum SSC from ~10 kg/m^3 to ~0.4 kg/m^3 as dispersion increases from 5 m^2/s to 500 m^2/s. Similarly, the ratio of the maximum bottom concentration ($C_{b,max}$) to c_* decreases from ~10 for $c_* = 0.2$ kg/m^3 to ~5 for $c_* =$ 20 kg/m^3, indicating that turbidity currents reduce the maximum concentration for large c_*.

Several factors cause an upstream movement of the turbidity maximum, including increasing settling velocity (Fig. 3c) and depth (Fig. 3e) and decreasing freshwater discharge (Fig. 3d) and vertical mixing (Fig. 3f). Decreasing the salinity gradient (increasing x_L; see Fig 3g) and an up-estuary shifting of the maximum salinity gradient x_c also cause an upstream migration of the turbidity maximum.

Because the estuary is funnel shaped, upstream movement of the turbid zone focuses sediment over a smaller cross-section, leading to an amplification of measured SSC. In particular, large increases in the SSC are observed as depth is increased from 5 to 10 m and as vertical mixing is decreased from 0.01 m^2/s to 10^{-4} m^2/s. The amplification effect, however, can be reduced when SSC is concurrently spread over a larger longitudinal area (see e.g. decreasing freshwater discharge in Fig. 3f from –80 m^3/s to –20 m^3/s or increasing settling velocity in Fig. 3c from 0.001 m/s to 0.01 m/s). Note that for some parameter values (e.g., large mixing or small settling velocity), the maximum sediment concentration occurs at the downstream model boundary.

As the turbidity maximum moves upstream, the distribution of SSC becomes more asymmetric (see for example the case of increasing depth, Fig 3e). Modelled estuaries whose width is strongly convergent (small L_e) display a relatively symmetric distribution of SSC, while more weakly convergent (large L_e) estuaries display a more asymmetric distribution

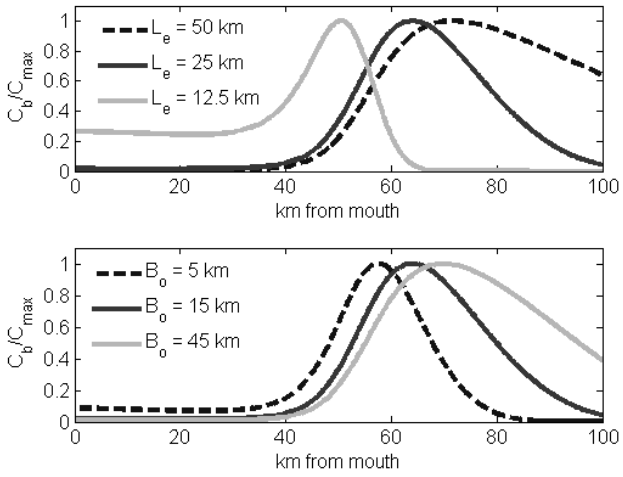

Figure 2. Sensitivity of modeled ETM to variations in the exponential width parameters L_e and B_o. The maximum SSC varies from 0.03 kg/m^3 (L_e = 50 km) to ~3.8 kg/m^3 (L_e = 12.5 km) in the top panel and from ~3.9 kg/m^3 (B_o = 5 km) to ~0.7 kg/m^3 (B_o = 45 km) in the bottom panel. The total mass in each model run is kept constant.

of SSC (Fig. 2a). The salinity gradient clearly controls the downstream extent of the turbid zone: sharp salinity gradients (small x_L) correspond with steep slopes in SSC, while gentle salinity gradients (large x_L) result in an increased downstream spread in SSC (Fig. 3g). Upstream of the turbidity maximum, a number of parameters such as Q, H, w_s, and A_v appear to affect the distribution of SSC.

3.2 *Scaling the turbid zone*

The observations in the sensitivity study suggest that we can construct length-scales that control the upstream and downstream extent of SSC. Using the result from Fig. 1, we assume that turbidity currents are negligible compared to dispersive fluxes (i.e., we neglect term 3 in Eq. 13b), and evaluate the remaining terms in Eq. 13.

Downstream of the turbidity maximum, the influence of freshwater discharge (term 2 in Eq. 13b) is small compared to gravitational circulation (term 1 in Eq. 13b), and can be neglected. By estimating the salinity distribution as a linear function ($s(x) \sim -S_* x/x_L$) we find that the e-folding lengthscale for the extent of the turbid zone downstream of the maximum is:

$$L_{SSC,d} \sim \frac{T_K K_h}{\frac{S_*}{x_L} T_s G_s} \approx \frac{Dispersive\ Influence}{Gravitational\ Influence} \qquad (15)$$

where $G_s = g\beta H^3/(48\rho_o A_v)$ scales the magnitude of gravitational circulation for a given salinity gradient. From this scaling, we find that factors which increase gravitational circulation –larger salinity gradients, greater depths, and decreased mixing—tend to decrease the downstream extent of the turbid

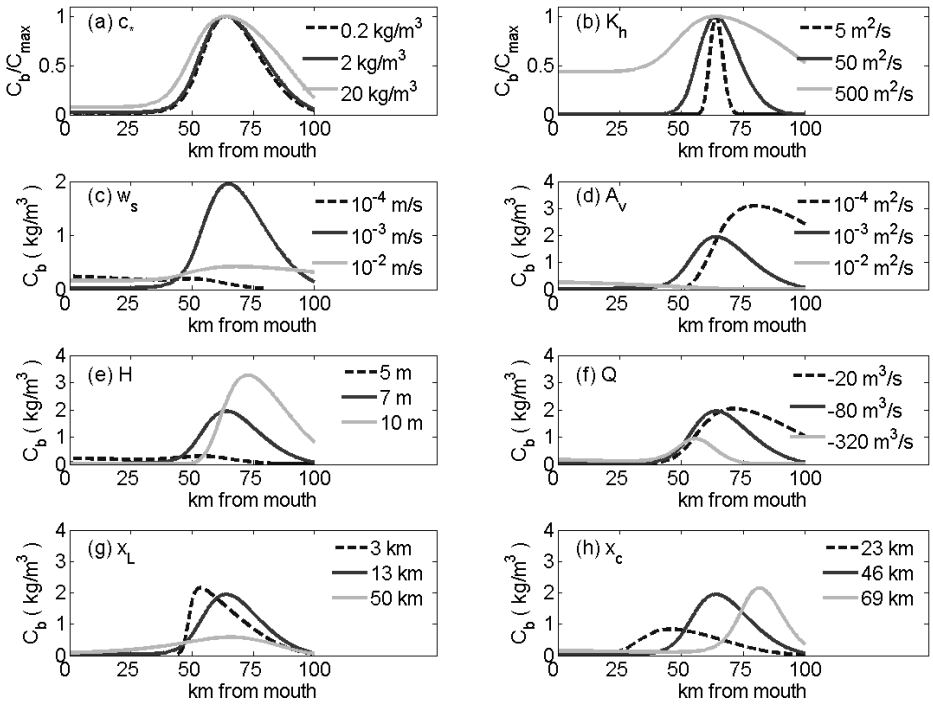

Figure 3: Variation of bottom SSC as a function of average sediment concentration c_* (3a), dispersion coefficient K_h (3b), the settling velocity w_s (3c), the eddy diffusivity A_v (3d), depth H (3e), freshwater discharge Q (3f), lengthscale of salinity gradient x_L (3g) and location of maximum salinity gradient x_c (3h). Panel (3a), (3b) and (3c) are normalized by the concentration at each turbidity maximum, while other results are presented in kg/m^3.

zone. Factors which increase horizontal dispersion (such as increased freshwater discharge) increase the size of the turbid zone downstream of the maximum.

The vertical distribution of sediment in the water column, defined by the vertical Peclet number $Pe_v = w_s H/K_v$, controls the downstream spread of turbidity through the ratio T_K/T_S. As shown in Fig. 4a, the ratio T_K/T_S is much larger than unity for small Peclet numbers. Essentially, because SSC is well mixed throughout the water column, the effect of gravitational circulation on sediment flux is reduced. As sediment settles towards the bottom with increasing Pe_v, near bottom gravitational currents become increasingly important, and the ratio T_K/T_S decreases to a minimum of ~2.5 at Pe_v =5.9. At higher Peclet numbers, the effect of the bed (u = 0) reduces fluxes from gravitational circulation relative to dispersion, and the ratio increases to 17.5 at Pe_v =100. Hence, this scaling suggests that there is a value of the settling velocity that minimizes the downstream extent of turbidity for a given depth and eddy diffusivity. For the standard parameter values in Table 1, this occurs for a settling velocity of $w_s \sim 8 \cdot 10^{-4}$ m/s.

When fresh water discharge dominates over gravitational circulation, as occurs upstream of the turbidity maximum (term 2 in Eq. 13b is larger than term 1), we find an approximate scale for the e-folding length-scale by first applying a Taylor expansion to the exponential width term in Eq. 13b around the location of the turbidity maximum, x_M:

$$\exp\left(\frac{x_a}{L_e}\right) \sim \exp\left(\frac{x_M}{L_e}\right)\left(1 + x_a/L_e + x_a^2/2L_e^2 + \ldots\right) \qquad (16)$$

where we introduce a new variable $x_a = x - x_M$. Using only the first two factors of Eq. 16 and substituting into Eq. 13b (i.e., discarding non-linear terms), we find that the function $F(x)$ from Eq. 13 becomes:

$$F(x) \sim \exp\left(\frac{-3T_Q|Q|L_e}{2HT_K K_h b_M}\right)\exp\left\{\frac{-x_a}{L_{ssc,u}}\right\} \qquad (17)$$

where the first term is a constant and the length $b_M = B_o \exp(-x_M/L_e)$ is the width at the turbidity maximum. The negative sign occurs because freshwater discharge is negative in our coordinate system. The e-folding lengthscale $L_{SSC,u}$, which scales the spread of SSC upstream of the turbidity maximum, is defined as:

$$L_{SSC,u} \sim \frac{2T_K K_h b_M H}{3T_Q|Q|} = \frac{Dispersive\ Influence}{Freshwater\ Influence} \qquad (18)$$

Factors which increase flux from freshwater circulation such as increased discharge or decreased width and depth tend to reduce the size of the upstream turbid zone. Factors which increase dispersion also increase the size of the turbid zone. To a first order, the width convergence length scale L_e does not affect the upstream e-folding lengthscale of SSC. However, the effect of width convergence enters the higher order terms in the Taylor expansion

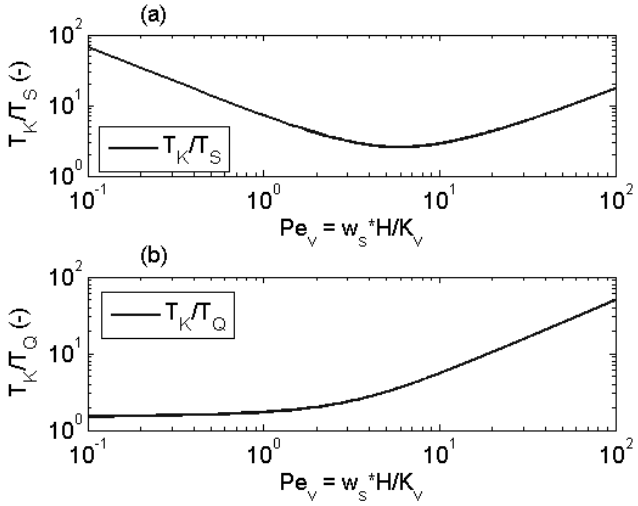

Figure 4. Variation of the ratio T_K/T_S and T_K/T_Q as a function of the vertical Peclet number Pe_v.

(Eq. 16). Hence, L_e adjusts the scaling in Eq. 18 in the manner observed in Fig. 2, which showed that small L_e (fast convergence) results in a reduced spread of SSC. Therefore, the scaling in Eq. 18 is an upper bound estimate of the upstream distribution of SSC for the case of constant width (large L_e).

The vertical distribution of SSC affects the upstream distribution of SSC through the ratio of T_K to T_Q, as is shown in Fig. 4b. As the Peclet number increases, the ratio of T_K to T_Q also increases from a value of ~ 1 at Pe_v =0.1 to a value of ~ 50 at Pe_v =100. This occurs because as sediment is concentrated near the bed, the sediment fluxes from freshwater discharge decrease relative to dispersion. Hence factors that increase the vertical Peclet number Pe_v such as increased settling velocity cause an increased upstream spread of sediment.

From the scaling estimates (Eq. 15 & 18) we can interpret the shapes of the turbidity profiles shown in Fig. 3. As readily observed in Eq. 15 & 18, increasing the salinity gradient (decreasing x_L) causes a sharp decrease in the extent of turbidity downstream of the turbidity maximum, but does not affect the upstream distribution (see Fig. 3g). By comparison, decreasing freshwater discharge Q clearly increases the upstream extent of turbidity, but has little effect on the downstream distribution (Fig 3f). Thus the differing parameters controlling the upstream and downstream portion of the turbidity zone inherently lead to asymmetry. Only the dispersion coefficient K_h and transport term T_K appear equally in both Eq. 15 & 18, and thus have an equal effect downstream and upstream of the maximum (see Fig. 3b).

3.3 Comparison with data

The dependence of the modelled profile of SSC downstream of the turbidity maximum on the applied salinity field downstream suggests that we compare measured longitudinal profiles of salinity with measured profiles of turbidity (proportional to SSC). Fig. 5 shows measured longitudinal profile of salinity (a) and turbidity (b) taken during 3 cruises on Sept. 28, 2005, Feb. 06, 2006, and Aug. 2, 2006 in the Ems estuary. Each cruise occurred during periods of low freshwater discharge between 25-40 m^3/s. The Sept. 28, 2005 measurement was an upstream cruise against the ebbing tide, the Feb. 2006 measurement was a downstream cruise against the flooding tide, while the Aug. 2006 cruise occurred in the downstream direction with the ebbing tide. Hence, the individual profiles of salinity and turbidity are either steepened (Sept. 2005 & Feb 2006) or lessened (Aug. 2006) compared to tidally averaged conditions. Nonetheless, it is useful to compare the shape and location of the salinity and turbidity profiles of each cruise to obtain insights into the relationship between the two. More details about measurement methods can be found in Talke et al., 2007.

As can be seen in Fig. 5, the turbid zone begins upstream of the largest salinity gradient and rises to a maximum at the toe of the salinity field. Confirming Eq. 1 and the explicit dependence of $C_b(x)$ on $s(x)$ in Eq. 13, we can fit a hyperbolic tangent to both the measured profiles of salinity and turbidity. The length scale parameter x_L in the hyperbolic fit to the turbidity curves is similar for all three measurements, and varies from 5.4 km (Sept. 2005) to 6.7 km (Aug. 2006). This is smaller than the length-scale x_L of the tidally averaged salinity profile for low-flow conditions in the Ems, which is ~ 14.5 km for a freshwater discharge of 30 m^3/s. Using S_* =25.3 psu, x_L = 14.5 km, and the standard values for settling velocity, depth, mixing, and dispersion coefficient (Table 1), we find that the e-folding length-scale for the modelled SSC in the downstream direction is ~ 5.4 km. Hence, the scaling in Eq. 15 gives the correct order of magnitude of the spread of turbidity downstream of the turbidity maximum.

We also scale the upstream spread of turbidity using Eq. 18. Estimating the width of the river to be ~ 350 m at the maximum at x = 70 km, we estimate an

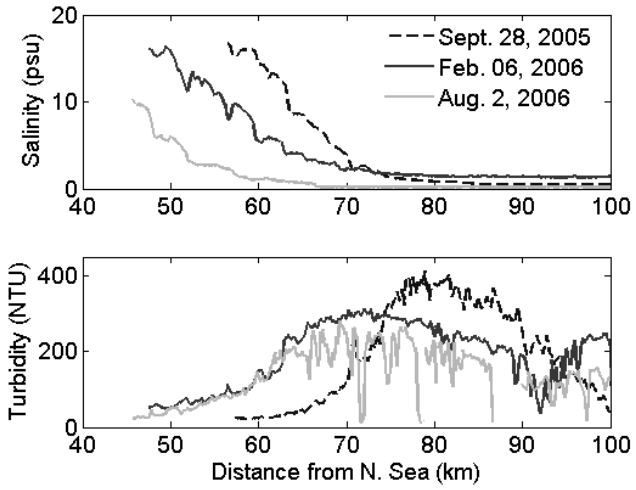

Figure 5. Comparison of salinity profiles (upper panel) and turbidity profiles (lower panel) in the Ems estuary. Practical turbidity units (NTU) are proportional to SSC.

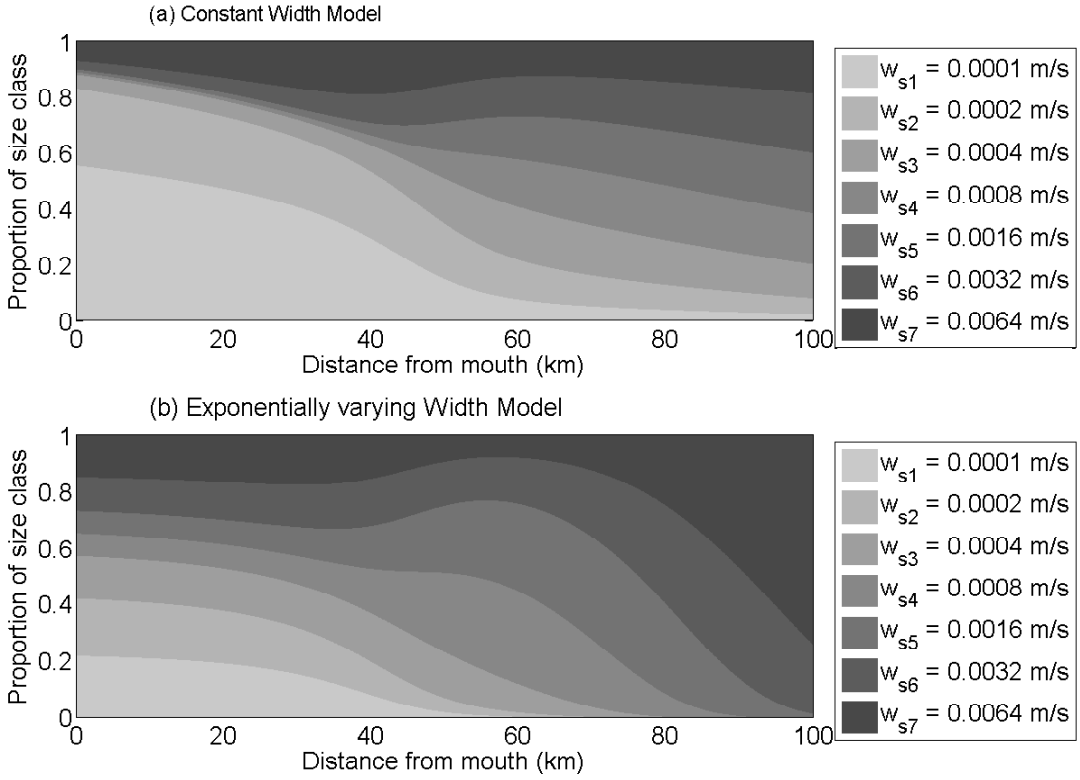

Fig. 6: Equilibrium distribution of settling velocities for constant width-model (6a) and exponentially converging width model (6b).

e-folding length-scale of turbidity to be ~22 km for the Feb. 2006 and Aug. 2006 cases. Similarly, the e-folding length-scale for Sept. 2005 is ~ 14 km. Though the measured extent of turbidity is larger (between 25-30 km), the scaling gives a good order of magnitude estimate. Moreover, the scaling from Eq. 15 and Eq. 18 are consistent with the observation that the spread of sediment is much larger in the upstream direction, and in this way explains the asymmetry of the turbidity zone.

3.4 *Distribution of particles*

As observed in Fig. 3c and shown by the scaling estimates in section 3.2, the longitudinal distribution of SSC in our model depends on the settling velocity of particles through the vertical Peclet number Pe_v Moreover, as settling velocity is increased, the position of the turbidity maximum is moved upstream (Fig. 3c). The dependence of the distribution of SSC on settling velocity provides a mechanism for the sorting of particles by settling velocity along the axis of an estuary. Starting with 7 particle sizes with settling velocities of 0.1, 0.2, 0.4, 0.8, 1.6, 3.2 mm/s, and 6.4 mm/s, and assuming that each is present in equal proportions (i.e., the c_* defined by Eq. 11 is equal), we calculate the equilibrium distribution of sediment for a constant width model (Fig. 6a) and an exponential width model (Fig. 6b). At each location along the longitudinal axis we plot the relative percentage of particles with a particular settling velocity to the combined concentration from all 7 settling classes. For simplicity, we assume that turbidity currents and hiding effects due to differing grain sizes are negligible.

When width is held constant (Fig. 6a), particles with small settling velocities are swept to the downstream boundary, while particles with larger settling velocities are trapped progressively further upstream. Approximately 83% of particles at the downstream boundary derive from the two smallest size classes (w_s =0.1, 0.2 mm/s) and ~ 62% of particles at the upstream boundary derive from the largest size classes (w_s =1.6, 3.2, and 6.4 mm/s). For an exponentially varying width, the particle size distribution of SSC in the upstream reaches becomes dominated by particles with large settling velocities: nearly 100% of the particles at the upstream boundary belong to the two largest settling velocity classes (see Fig. 6b). By contrast, the distribution of particles in the downstream reaches becomes more evenly distributed. At the boundary, ~35% of the distribution reflects sediment from the three largest size classes (w_s =1.6, 3.2, and 6.4 mm/s), compared to ~11 % for the constant width model. In both the constant width model and the exponential model, a large shift in the distribution of settling velocities occurs between 40 km to 70 km, with settling velocity becoming larger. This shift coincides with the maximum salinity gradients prescribed in the model, and demonstrates the effect of gravitational circulation on SSC spreading downstream of the turbidity maximum (see Eq. 15 and Fig. 4a).

At first glance the distribution of particles predicted by the model is contradicted by observations, which show that large grained sands (large settling

velocities) are found in the outer estuary while silt (small settling velocity) is found trapped at the turbidity maximum. However, because flocculation of cohesive sediments increases the effective settling velocity to 0.5-3 mm/s (see Sanford et al., 2001 and Winterwerp, 2002), the modelled settling velocities in the turbid zone (see Fig. 6) between km 50 and km 90 are consistent with settling velocities at turbidity maximums. As in the model results, particles with small settling velocities are not found in turbidity zones; for example, Sanford et al. (2001) found no turbidity maximum in the Chesapeake when settling velocity reduced to $\sim 3 \cdot 10^{-4}$ m/s during the winter months. Though particles with small settling velocities are not measured in the field along the main axis of an outer estuary, it is possible that these particles are trapped at mudflats along the embankments by lateral circulation processes (see e.g. Huijts et al., 2006, Fugate et al. 2007). It is also possible that these small particles are swept to sea by processes not considered in this model but that may be relevant in an outer estuary (tides, winds, and transient, non-equilibrium processes).

4 CONCLUSIONS

In this paper we derive an implicit solution for the distribution of SSC in an estuary with an exponentially varying width. Results show that turbidity currents can be neglected for all but the muddiest estuaries. A sensitivity study shows that increasing depth and settling velocity moves the turbid zone upstream, while increased mixing and freshwater discharge move the turbid zone downstream. Strongly convergent width results in a smaller spatial extent of SSC. Length-scales were derived that control the modelled distribution of SSC, and are shown to depend greatly on the prescribed salinity field, freshwater discharge, depth, settling velocity, and other model parameters. The modelled variations in settling velocity were used to determine the distribution of particles with different settling velocities. The settling velocities found in the turbid zone are consistent with reported values of the settling velocity of cohesive sediments. In the future, the model will be further improved by allowing more parameters to be functions of the longitudinal coordinate, and by allowing tidal motions (for a discussion of the limitations of a tidally averaged model, see Talke et al., 2007).

4.1 *Acknowledgements*

This work was funded by LOICZ project 014.27.013 (Land Ocean Interaction in the Coastal Zone), and administered by NWO-ALW, the Netherlands Organization for Scientific Research.

5 REFERENCES

Festa, J.F. & Hansen, D. V., 1978. Turbidity maxima in partially mixed estuaries: A two dimensional numerical model. *Estuarine and Coastal Marine Science*, **7**, 347-359.

Fugate, D.C., Friedrichs, C.T., & Sanford, L.P., 2007. Lateral Dynamics and associated transport of sediment in the upper reaches of a partially mixed estuary, Chesapeake Bay, USA. *Continental Shelf Research*, **27**, 679-698.

Hansen, D.V. & Rattray Jr., M., 1965. Gravitational circulation in straits and estuaries. *Journal of Marine Research* **23**, 104-122.

Huijts, K.M.H, Schuttelaars, H.M., de Swart, H.E. & Valle-Levinson, A., 2006. *Journal of Geophysical Research* **111**, F02013, doi:10.1029/2005JF000312.

Officer, C.B., 1976. *Two dimensional density gradient flow*. Physical oceanography of estuaries (and associated coastal waters): 125-129. New York: Wiley.

Sanford, L.P., Suttles, S.E. & Halka, J.P., 2001. Reconsidering the physics of the Chesapeake Bay estuarine turbidity maximum, *Estuaries*, **24** (5), 655-669.

Sottolichio, A., & Castaing, P., 1999. A synthesis on seasonal dynamics of highly concentrated structures in the Gironde estuary, *Surface Geosciences*, **329**, 795-800.

Winterwerp, J.C., 2002. On the flocculation and settling velocity of estuarine mud, *Continental Shelf Research*, **22(9)**, 1339-1360.

6 APPENDIX

The expressions T_s, T_t, T_Q, and T_K are defined as described in Talke et al., 2007, and are functions of the vertical Peclet number for suspended sediment concentration $Pe_v = w_s H/K_v$:

$$T_s = \frac{1}{Pe_v^{\,4}} \left\{ \begin{array}{l} \left(-48 + Pe_v^{\,3} - 18 Pe_v\right) \exp\left(-Pe_v\right) + \\ 48 - 30 Pe_v + 6 Pe_v^{\,2} \end{array} \right\} \qquad \text{(A.1)}$$

$$T_T = 144 Pe_v^{\,-7} \exp\left(-2Pe_v\right) \left\{ \begin{array}{l} -1 + \frac{1}{12} Pe_v^{\,4} + Pe_v^{\,2} + \frac{1}{2} Pe_v^{\,3} + \\ \left(-2Pe_v - Pe_v^{\,2} + \frac{1}{3} Pe_v^{\,3} + 2\right) \exp\left(Pe_v\right) + \\ \left(-1 - Pe_v^{\,2} + \frac{1}{6} Pe_v^{\,3} + 2Pe_v\right) \exp\left(2Pe_v\right) \end{array} \right\} \qquad \text{(A.2)}$$

$$T_Q = \frac{-2}{Pe_v^{\,3}} \left\{ \left(-1 + \frac{1}{2} Pe_v^{\,2}\right) \exp\left(-Pe_v\right) + 1 - Pe_v \right\} \qquad \text{(A.3)}$$

$$T_{K_h} = \frac{\left(1 - \exp\left(-Pe_v\right)\right)}{Pe_v} \qquad \text{(A.4)}$$